Photochemical & Photobiological Sciences

COMMUNICATION

Ni/Co/Ti layered double hydroxide for highly efficient photocatalytic degradation of Rhodamine B and Acid Red G: a comparative study†

Received 25th January 2017,
Accepted 17th April 2017
DOI: 10.1039/c7pp00030h
rsc.li/pps

Priyadarshi Roy Chowdhury * and Krishna G. Bhattacharyya *

Optically responsive, luminescent Ni/Co/Ti layered double hydroxide (LDH), synthesized by a single step hydrothermal route, exhibits highly efficient photodegradation of cationic and anionic dyes, Rhodamine B (~99.8%) and Acid Red G (~99.6%) respectively, better than that of commercial catalysts like NiO, CoO and TiO_2. The LDH has been characterized by using XRD, XPS, PL, TRES, EIS, TEM, SEM-EDX, AFM, UV-visible DRS, N_2-sorption desorption, ξ-potential, FT-IR and TG techniques. The characterized results indicate that the LDH possesses hexagonal morphology, a high surface area, a narrow band gap, defect states and oxygen vacancies within its layered framework. The degradations follow the e^-–h^+ hopping pattern and dye-photosensitized mechanistic pathways. The active species generated during photocatalysis have been evaluated using ESR, terephthalic acid fluorescence probe and indirect radical–hole trapping experiments. The colourless end products were investigated by GC-MS and reaction mechanisms have been established for the degradation of the dyes to less toxic and more eco-friendly molecules than their parent analogues. Dye mineralization studies (performed using a TOC analyser) and closure of carbon mass balance experiments quantified the amount of carbon entering and leaving the reaction systems. Reaction mechanisms have been proposed on the basis of the asymmetric cleavage of the dyes. The LDH demonstrated its remarkable efficiency in the field of waste water treatment.

Dyes are the primary sources of coloured organics that are extensively used in the textile industry. The discharge of dyes in effluents at comparatively high concentrations makes their removal difficult through conventional processes like filtration, coagulation, biological oxidation and adsorption on activated carbon *etc.* Hence, it is very important to develop simple and economical techniques for the removal of these hazardous substances from water. At present, visible light induced photocatalysis is of great interest because of its ability to degrade a wide variety of organics and dyes.[1–4]

Layered double hydroxides (LDHs) represent a hydrotalcite category of nanomaterials that have attracted interest due to their unique semiconducting properties. The unique properties of LDHs could be attributed to their layered structure, narrow band gap and existence of different surface states of metals accompanied by oxygen vacancies.[5,6] Their general formula is $[M^{2+}_{1-x}M^{3+}_{x}(OH)_2](A^{n-})_{x/n}\cdot yH_2O$, where M^{2+} and M^{3+} represent divalent and trivalent cations, and A^{n-} is the charge balancing interlayer anion. Titanium containing LDHs have received importance due to their remarkable ability in waste water treatment. The present work illustrates the highly efficient photo-assisted degradation of cationic and anionic dyes, Rhodamine B (RhB) [Fig. S1; ESI†] and Acid Red G (ARG) respectively [Fig. S2; ESI†] with 2 : 1 : 1 Ni/Co/Ti LDH, carried out using a specially designed photocatalytic device [S12; Fig. S13(A); ESI†]. The main objective of this work is to examine the important parameters associated with photocatalysis of the test dyes. The LDH exhibited superior performance with respect to degradations of both the dyes, over commercial catalysts like NiO, CoO and TiO_2. The degradations follow pseudo-first order kinetics, e^-–h^+ hopping conduction and dye-photosensitized mechanistic pathways. The decolorized end products were analysed using GC-MS and reaction mechanisms have been proposed on the basis of the asymmetric cleavage of the dyes.

2 : 1 : 1 Ni/Co/Ti LDH has been synthesized by a hydrothermal route, taking 10.98 g $Ni(NO_3)_2\cdot6H_2O$, 5.65 g $Co(NO_3)_2\cdot6H_2O$, 1.1 ml $TiCl_4$ and 3.0 g urea in 100 ml decarbonated water, followed by vigorous stirring of the mixture and subsequent hydrothermal ageing in an autoclave at 130 °C for 48 h. The crystalline product so formed was extracted, washed with decarbonated water and dried. The synthesis procedure is schematically illustrated in S2 (ESI†).

The characterization techniques associated with this work are presented in S3 (ESI†). The XRD pattern (Fig. S4; ESI†) of the LDH shows the characteristic Bragg's reflections associated

Department of Chemistry, Gauhati University, Guwahati-781014, Assam, India. E-mail: priyadarshiroychowdhury@yahoo.in, kgbhattacharyya@gmail.com; Fax: +91 3612570599; Tel: +91 9435249993, +91 9864031987

† Electronic supplementary information (ESI) available: Characterization, photo-assisted degradations, mechanistic pathways and reaction mechanisms of degradations of the dyes with Ni/Co/Ti LDH. See DOI: 10.1039/c7pp00030h

with the hexagonal phase having interlayer CO_3^{2-} ions, similar to the previously reported X-ray diffraction data for LDHs.[2,3] A well-defined series of (00*l*) Bragg reflections shows the existence of a parallel house-of-cards type of stacking of brucite sheets. The existence of the (003), (006) and (009) reflections at 2θ values of 13.42°, 26.56° and 41.05° respectively indicates the incorporation of CO_3^{2-} ions and H_2O molecules within the LDH lattice. The *d*-spacing corresponding to the (003) peak was found to be 0.664 nm and that of (110) was 0.313 nm ($2\theta \approx 28.56°$). Since the basal spacing of the synthesized LDH is similar to that of Ti incorporated LDHs, it is most likely that the interlayer CO_3^{2-} and H_2O molecules have retained a pattern, similar to that of the previously reported X-ray diffraction data for LDH materials. Moreover, the existence of the (110) and (101) diffraction planes at 2θ values of 28.56° and 37.43° indicates the existence of TiO_2 in the anatase phase within the synthesized LDH.[3] The narrow and sharp diffraction peaks represent good crystallinity. The other diffraction peaks like (018), (100), (01$\underline{1}$1), (113) and (10$\underline{1}$3) could be indexed to typical LDHs with interlayer CO_3^{2-} ions and H_2O molecules. The XRD parameters are illustrated in Tables S1 and S2 (ESI†). The high resolution TEM micrographs [Fig. 1(A and B)] of the LDH revealed ultra-fine hexagonal nanoparticles, stacked one over the other, in good agreement with SEM observations [S5; ESI†]. The SAED pattern [Fig. 1(C)] exhibits good hexagonal arrangement of the diffraction planes for the in-plane symmetry, intrinsic to the LDH layers, showing the house-of-cards type of stacking of the hetero-layered LDH crystallites. The distance between the lattice fringes from the (110) plane of the nanomaterial, investigated by TEM analysis [Fig. 1(D)], was approximately 0.313 nm, exactly matching the value obtained from the X-ray diffraction studies (Table S1; ESI†). The average particle size was found to be 100 nm, calculated from the histogram plot [Fig. 1(E)]. Furthermore, the cross sectional TEM image [Fig. 1(F)] revealed the distance between two consecutive parallel metal hydroxide layers to be 0.671 nm (0.289 nm + 0.382 nm) for the synthesized Ni/Co/Ti brucite sheets, matching the *c*′ lattice parameter observed in the XRD studies (Table S2; ESI†). This estimated interlayer distance consists of a brucite sheet thickness of 0.382 nm and an interlayer thickness of 0.289 nm, as evident from Fig. 1(F). EDX analysis reveals Ni/Co/Ti atomic and weight ratios to be 2.03 : 1.02 : 1, thereby matching the nominal stoichiometric ratios of Ni, Co and Ti used during synthesis (Table S3; ESI†). The EDX spectrum is presented in Fig. S4(B) of the ESI†.

Tapping mode atomic force microscopy (AFM) analysis was also performed to determine the morphology and total thickness of the LDH nanosheets (Fig. S6; ESI†). The AFM micrographs [Fig. S6(A, C, D); ESI†] also confirm the existence of hexagonal platelets, possessing 120° internal angles, consistent with the SEM and TEM observations. The flat terrace [Fig. S6(B); ESI†] in the AFM height profile provides strong evidence for the existence of parallel brucite sheets. The brucite sheets are aligned parallel to each other within the substrate to maximize the attractive energy. The total thickness of Ni/Co/Ti LDH along the *c*-axis [Fig. S6(C); ESI†] is determined to be 23 nm. The thickness of a single hexagonal crystallite [Fig. S6(D); ESI†] is found to be approximately 0.382 nm [Fig. S6(B); ESI†], which is in good agreement with that obtained from the cross sectional TEM results [Fig. 1(F)]. On dividing the total thickness by the *c*′ lattice parameter (calculated using the XRD data; Table S2; ESI†), it is observed that the LDH consists of 34–35 layers of parallel brucite sheets. The AlK_α XPS survey spectrum reveals the existence of elements in different chemical states on the LDH surface. XPS indicates the presence of Ni in its (0) and +(II) states in the LDH. Moreover Ti is present in +(III) and +(IV) states, whereas Co is present in +(II) and +(III) states respectively. Meanwhile, the O 1s XPS scan reveals the existence of the corresponding oxides of different metals present on the LDH surface. The deconvoluted spectra confirm the existence of mixed valency of metals, along with the nature of bonding of the constituent elements in the LDH. The existence of mixed valency indicates the possibility of occurrence of a series of redox reactions on the LDH surface, assisted by visible light, which degrades complex organic dyes to colourless molecules.[3] (The experimental details of XPS are available in S7; ESI†).

The N_2 sorption–desorption measurements at 77 K revealed a Type IV isotherm [Fig. S9(A); ESI†] with a H3-type hysteresis loop (at P/P_0 > 0.4–0.8) indicating the condensation of N_2 within the pores and its release with reduced pressure followed different paths, a characteristic property exhibited by mesoporous materials. A specific surface area of 168 $m^2\ g^{-1}$ with a pore width of 4.0 nm [Fig. S9(B); ESI†] is observed for the LDH. This could be attributed to the use of urea as the basic

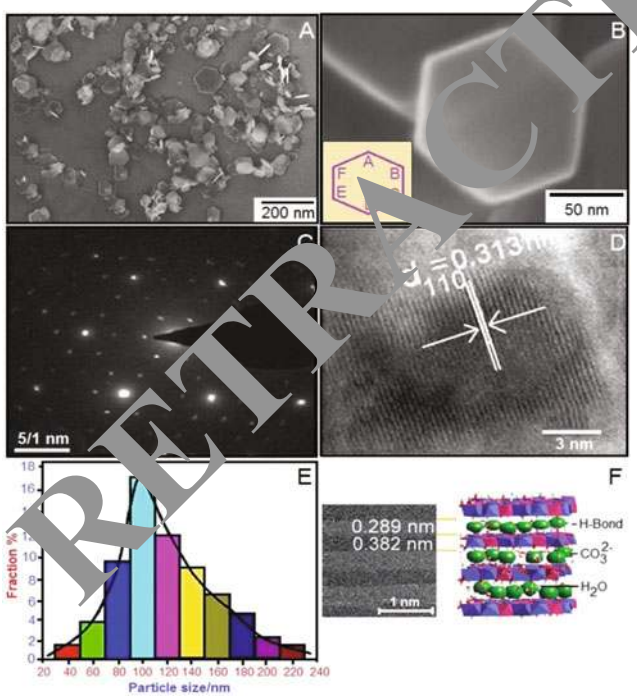

Fig. 1 (A, B) HR-TEM images, (C) SAED pattern, (D) TEM image showing lattice fringe separation from the (110) plane, (E) histogram plot showing particle size distribution, (F) cross-sectional TEM micrograph showing co-relation with the idealised structure of Ni/Co/Ti LDH.

precipitant during LDH synthesis. The LDH is dominated by both micropores and mesopores, with diameters ranging between 1 and 5 nm. The mesoporous nature of the material with an appropriate network of pores assists in the e^-–h^+ transfer throughout the layered framework, thereby contributing to its high photocatalytic performance.[2]

Electrochemical impedance spectroscopy (EIS) analysis, performed using a three electrode electrochemical workstation, with a 2.5 mM $K_3[Fe(CN)_6]/K_4[Fe(CN)_6]$ (1 : 1) mixture in 0.5 M aqueous Na_2SO_4 solution as the redox probe, indicated a decrease in the solid interface layer resistance and charge transfer resistance on the LDH electrode. The high charge transfer efficiency is indicated by the small arc radius of the electrochemical impedance Nyquist plot [Fig. S9(C); ESI†]. Meanwhile, the Mott-Schottky (MS) impedance measurements yielded a reversed sigmoid curve that indicates that the LDH has n-type semiconductor properties [Fig. S9(D); ESI†]. The flat band potential (V_{fb}) obtained from the *x*-intercept of the linear region of the MS plot was observed to be −0.78 V *vs.* SCE. The negative V_{fb} potential suggests the presence of different surface states that have led to a considerable change in its band positions. The existence of different surface states of the metals within the LDH has been found to be in accordance with the XPS results. The conduction band potential (E_{CB}) of the n-type semiconductor lies in the range between −0.2 and 0 V, close to the V_{fb} value observed for the LDH. The flat band potential mainly depends on the effective electronic mass and carrier concentration. In this case, the voltage difference between the conduction band and the flat band is set at 0.1 V. Thus, the Fermi level causes E_{CB} to lie at −0.78 V *vs.* SCE. The negative value of E_{CB} imparts a strong reducing power to the LDH.[2] Since the standard redox potential of $O_2/O_2^{\bullet-}$ (−0.41 V *vs.* SCE) is less negative than the E_{CB} of the LDH, it suggests that the photo-generated electrons could theoretically react with adsorbed O_2 to form $O_2^{\bullet-}$ species. The overall transporting properties of the LDH could be attributed to the suppression of charge pair recombination being supported by the photoluminescence results. Thus, the enhanced photodegradation of the dyes with the LDH could be attributed to the charge-pair separation, extended photo-responding range, negative flat-band potential and high migration efficiency of the photo-induced electrons.

The thermogravimetric (TG) curve of the LDH showed [Fig. S10(A); ESI†] three degradation steps. The first weight loss at 98 °C could be attributed to the removal of physisorbed and interlayer water constituting ~14% by weight; the second weight loss at 291 °C accounted for 15% loss, due to the concomitant dehydration of the brucite layers; and the third weight loss of ~18.5% observed at 388 °C could be due to the decomposition of the interlayer CO_3^{2-} anions.[3]

The FT-IR spectra showed characteristic frequencies that represented the existence of H_2O and CO_3^{2-} in the interlayer galleries of the LDH [Fig. S10(B); ESI†].[2,3] The results of the FT-IR analysis are presented in S9(i) of the ESI.†

Photoluminescence (PL) analysis indicated the separation of e^-–h^+ pairs, the lifetime of charge carriers and the existence of shallow and deep trap defects on the LDH surface which plays a vital role in photocatalysis.[3] The PL excitation spectra determined the appropriate excitation wavelength necessary for the generation of charge carriers that assist in the photodegradation. The experimental results of PL and its associated mechanism are shown in S10 (ESI†).

The UV-visible DRS of the LDH showed a broad absorption band extended over the entire visible region.[1–3] Commercial photocatalysts like NiO, CoO and TiO_2, however, showed absorption between 250 and 450 nm [Fig. S12(A); ESI†]. The enhanced absorbance in the visible region imparted better photocatalytic properties to the LDH in comparison to the commercial photocatalysts. Meanwhile, the LDH exhibited a comparatively narrower direct band gap of 2.1 eV (= E_g) than that of the commercial photocatalysts [Fig. S12(B); ESI†]. The band gap is calculated using the classical Tauc equation, presented in eqn (1):

$$\alpha h\nu = K(h\nu - E_g)^n \quad (1)$$

where E_g represents the optical band gap, $h\nu$ is the photon energy, K is a constant and n = 1/2 for direct allowed transitions. The band gaps of 2.68 eV, 3.18 eV and 3.26 eV were observed respectively for CoO, NiO and TiO_2. The narrow band gap of the LDH is mainly responsible for its highly efficient photocatalytic performance. The results of the UV-visible DRS analysis are shown in S11 (i, ii) and Fig. S12(A, B) of the ESI.† The ξ-potential measurements, performed between pH 4 and 11, revealed variation of electrical surface charge with the pH of the LDH [Fig. S12(C); ESI†]. The surface charge of the LDH decreased monotonically on increasing the pH, thereby attaining point zero charge at pH 7.93, which could be identified as the isoelectric point of the LDH. Thus, the cationic dye RhB and the anionic dye ARG would be electrostatically attracted to the LDH surface at pH > $pH_{(zpc)}$ and pH < $pH_{(zpc)}$ respectively, leading to its higher photodegradation efficiency.[3] The photocatalytic efficiency of the LDH was evaluated with cationic RhB and anionic ARG dyes separately in aqueous medium, by dispersing the LDH in 200 ml dye solution, followed by vigorous stirring of the mixture for 30 min in the dark for establishing adsorption–desorption equilibrium [Fig. S13(B); ESI†], followed by visible light irradiation. The dye solutions were rendered colourless on irradiation for 60 min. Aliquots were taken at 10 min intervals, centrifuged and the centrifugate was analysed for the dye with an UV-visible spectrophotometer. The decrease in absorption intensities to nearly zero marked the end of the decolorization process with both the cationic and anionic dyes [Fig. 2(A and B)]. The photodegradation experiments were monitored with respect to the catalyst dose, pH, initial dye concentration and effects of scavengers. The maximum efficiency was observed for 1×10^{-5} M dye concentration (S12.3; ESI†) with an LDH dose of 15.0 mg (S12.1; ESI†). The ARG dye showed a maximum of ~99.6% degradation efficiency at pH 4, whereas RhB showed ~99.8% degradation at pH 11 after 60 min visible light irradiation (S12.2; ESI†). The LDH remained stable up to the fifth catalytic cycle

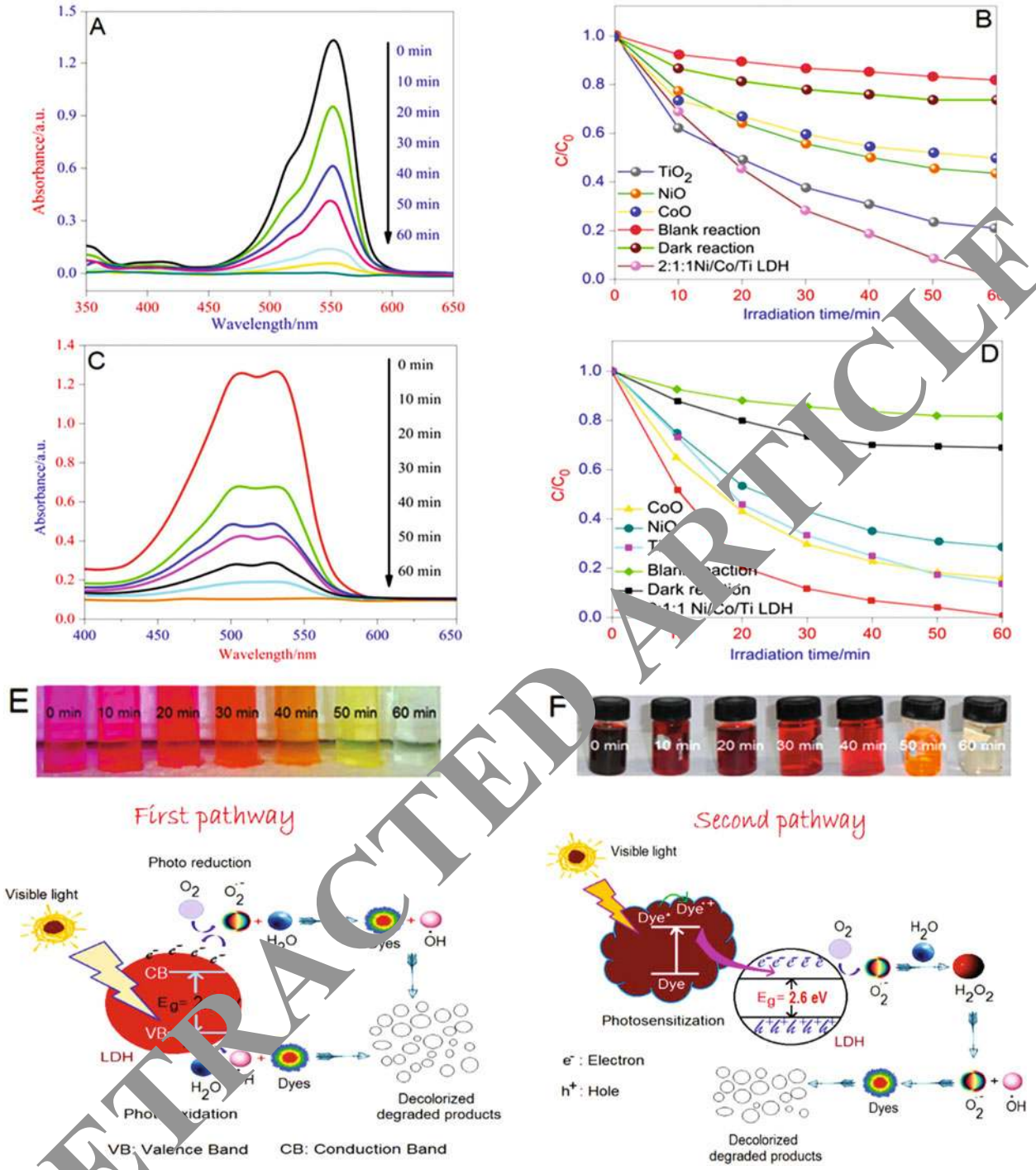

Fig. 2 [illegible] visible [illegible]sorption spectra of (A) ARG and (C) RhB with Ni/Co/Ti LDH at every 10 min intervals. Comparative degradations of aqueous (B) R[illegible]B an[illegible](D) ARG using Ni/Co/Ti LDH under visible light and control conditions and commercial catalysts. (E, F) Snapshots of the aliquots taken at differ[illegible]ervals for the photodegradations of RhB and ARG with Ni/Co/Ti LDH. Mechanistic pathways of photodegradation by Ni/Co/Ti LDH based o[illegible]athway 1) the e^{-}–h^{+} hopping conduction model and (Pathway 2) photosensitization of dyes.

for both the dyes. Even in the fifth cycle, the degradation was found to be 91% for RhB and 90% for ARG, indicating a good recyclability of the LDH for the degradations [Fig. S17; ESI†]. The FT-IR analysis of the LDH recovered after the fifth cycle (with both the dyes) showed the existence of all the major FT-IR bands in their respective positions [Fig. S18(A and B); ESI†]. The kinetics was found to agree with the pseudo first order model for both the dyes. The calculated half-life for the degradation was 10.83 min for ARG and 16.91 min for RhB. The rate constant (k_{app}) was 0.064 min^{-1} for ARG and

Table 1 Comparative degradation of aqueous RhB and ARG

	Degradation efficiency (%)	
Reactions with	RhB	ARG
Ni/Co/Ti LDH	99.8	99.6
TiO_2	78	84
NiO	57	70
CoO	50	83
Blank	19	18
Dark	23	27

0.041 min^{-1} for RhB [the results are presented in S12.6; (ESI†)].

The roles of active species in the degradations were investigated to establish the mechanistic pathways of degradations. The presence of $^{\bullet}OH$ species was evaluated by using the terephthalic acid (TA) fluorescence probe and $O_2^{\bullet-}$ by the EPR technique. The role of active species like $^{\bullet}OH$, h^+ and $O_2^{\bullet-}$ was also evaluated indirectly by external addition of quenchers like *n*-butanol (a hydroxyl radical ($^{\bullet}OH$) quencher), disodium ethylenediaminetetraacetate (2Na-EDTA) which is a quencher for photogenerated holes (h^+) and benzoquinone (BQ, a superoxide $O_2^{\bullet-}$ quencher) to the experimental mixtures at the beginning of the photocatalysis. The suppression of degradations indicated that $^{\bullet}OH$, h^+ and $O_2^{\bullet-}$ were the active species involved in the dye degradations [the details are available in S12.7; (ESI†)].

A comparative photocatalytic study of RhB and ARG [Fig. 2 (B and D)] showed a higher photocatalytic efficiency of the LDH over that of commercial NiO, CoO and TiO_2. Control experiments (blank and dark reactions) showed negligible efficiency, indicating that the dye degradations are controlled only by visible light. The results are presented in Table 1.

A comparative FT-IR analysis of the end products of control experiments and photocatalytic reactions [S12.8; (ESI†)] showed the dominance of adsorption in the control experiments whereas degradation and decolorizations of the dyes marked the end of photocatalytic experiments [Fig. 2(E and F)]. Thus, on the basis of the results of XPS, PL, EIS, EPR, terephthalic acid fluorescence probe and indirect radical and hole trapping experiments, mechanistic pathways of dye degradations by the LDH have been proposed taking its O 1s orbital as the valence band and Ni-2p, Co-2p and Ti-2p orbitals as the conduction band. Photocatalysis has been found to proceed *via* e^-–h^+ hopping (pathway 1) and by photosensitization of the dyes (pathway 2). The series of sequential reactions associated with the mechanistic pathways is illustrated in S12.9 (ESI†). The decolorized end products were identified with GC-MS; and the reaction mechanism is elucidated for the mineralization of the complex dyes to simple and less toxic molecules than the parent dyes (S12.10; ESI†). The extent of total organic carbon (TOC) removal was observed to be 94% for the RhB metabolite and 88% for the ARG metabolite (S.12.11; ESI†). The TOC removal rate shows that the complex dyes have been degraded to simpler molecules than their parent analogues. Meanwhile, carbon mass balance experiments revealed a complete closure of the carbon mass balance, indicating that the dyes have been mineralized through a relatively rapid pathway.

Conclusions

Thus, Ni/Co/Ti LDH played a remarkable role in the photocatalytic degradations of both cationic and anionic dyes in aqueous media. This could be attributed to the existence of high specific surface area, narrow band gap, defects and oxygen vacancies within the layered framework. The photocatalytic performance of the LDH has been observed to be remarkable in comparison to that of commercial NiO, CoO and TiO_2. The mechanistic pathways involve e^-–h^+ hopping and photosensitization of the dyes. The end product analysis and the mineralization studies revealed that the complex dyes have been completely degraded to simple molecules, suggesting that LDH could be used as a cost-effective and recyclable photocatalyst for environmental wastewater treatments.

Acknowledgements

PRC is thankful to the Council of Scientific and Industrial Research (CSIR), India, for providing financial assistance under the CSIR-SRF scheme.

References

1 N. Zhang, M. Q. Yang, S. Liu, Y. Sun and Y. J. Xu, *Chem. Rev.*, 2015, **115**, 10307.
2 P. Roy Chowdhury and K. G. Bhattacharyya, *RSC Adv.*, 2016, **6**, 112016.
3 B. Liu, K. Nakata, M. Sakai, H. Saito, T. Ochiai, T. Murakami, K. Takagi and A. Fujishima, *Catal. Sci. Technol.*, 2012, **2**, 1933.
4 G. Chen, S. Qian, X. Tu, X. Wei, J. Zou, L. Leng and S. Luo, *Appl. Surf. Sci.*, 2014, **293**, 345.
5 S. Kim, J. Fahel, P. Durand, E. André and C. Carteret, *Eur. J. Inorg. Chem.*, 2017, 669.
6 Q. Wang and D. O'Hare, *Chem. Rev.*, 2012, **112**, 4124.